


Carrier Localization by a Quantum Dot in a Quantum Well

A.N. Kosarev^{1,2,*} and V.V. Chaldyshev^{1,†}

¹*Ioffe Institute, 26 Politekhnicheskaya str., Saint Petersburg 194021, Russia*

²*Peter the Great Saint Petersburg Polytechnic University, 29 Politekhnicheskaya str., Saint Petersburg 195251, Russia*

 (Received 21 July 2021; accepted 8 October 2021; published 25 October 2021)

We show that a self-organized quantum dot (QD) embedded in a quantum well (QW) can provide better carrier localization compared to the bare QD due to a complex action of three processes, namely, an increase in the QD volume, a change of the QD aspect ratio, and strain redistribution provided by the QW. For an InAs QD and an (In,Ga)As QW, we calculate the possible energy benefits of these three contributions and examine the optimal dot-in-well configuration sustaining the interface coherency.

DOI: [10.1103/PhysRevApplied.16.044046](https://doi.org/10.1103/PhysRevApplied.16.044046)

A capability to localize charge carriers in all three dimensions is the key property of semiconductor quantum dots (QDs). When the QDs are produced via self-organization in the process of the commercial semiconductor growth technologies, which are molecular-beam epitaxy and metalorganic chemical vapor deposition, they can be utilized in a variety of semiconductor devices, such as lasers, light-emitting diodes, solar cells, memories, and others [1,2]. In the research and development of quantum computing, the QDs are excellent candidates for ultrafast coherent manipulation of qubits [3,4].

Most popular self-organized QDs are based on the GaAs-InAs material system. The InAs QDs are attractive for many applications listed above due to the well-developed growth technology and the ability to localize both electrons and holes. In fact, the band gaps of GaAs and InAs at room temperature are 1.42 and 0.35 eV, respectively [5], with the band offset $\Delta E_c/\Delta E_g = 0.83$ [6]. The InAs QDs are apparently tunable over a very wide optical range, including common telecommunication bands. Unfortunately, the very wide tunability of the QDs is delusive.

While a blueshift of the optical emission from the QD can be achieved by making them smaller at the self-organization stage or by intermixing via postgrowth annealing [7], the redshift is much more problematic. The depth of carrier localization is substantially limited by the mechanical stress-strain field originated from the lattice mismatch, which is required for the self-organization process [8]. In addition, it sets the upper limit on the volume of QD with coherent (dislocation-free) interfaces [9].

In the case of InAs QDs in GaAs the described limitation sets the longest emission wavelength near 1.1 μm . Deep carrier localization is critical for most applications to prevent thermal evaporation of the localized carriers from the QDs to the barriers. Within the bounds of the interface coherency, the carrier localization in the QD of a given volume can be somewhat improved by an optimization of the shape and aspect ratio [10].

The carrier localization can be enhanced with a substantial redshift of the optical emission, if the QD is embedded into a quantum well (QW). Such a structure is referred to as DWELL. It was experimentally shown by Ustinov and co-workers [11] and by Nishi and co-workers [12] that the optical emission from the InAs QDs can be redshifted to 1.3 μm , if the QD is embedded into an (In,Ga)As QW.

These initial observations were followed by a large number of papers, see, for instance, Refs. [13–19], in which the phenomenon of DWELL was examined experimentally and by simulations. It was shown that the redshift of the excitonic optical emission from the InAs depends on the geometry of the QD, as well as the thickness and chemical composition of the QW. It is interesting to point out that experimental optimization of the DWELL parameters has led to similar results by numerous independent research groups. Namely, the largest experimentally achieved redshifts for the optical emission from the InAs DWELL compared to the InAs QD in bulk GaAs are 160 [11], 140 [12], 130 [20], 160 [21], 120 meV [22].

There are two different explanations for the phenomenon. Ustinov *et al.* [11] observed a certain increase of the base of the pyramidal InAs QDs as a result of capping by the (In,Ga)As QW. Then,

*kosarev@mail.ioffe.ru

†chald.gvg@mail.ioffe.ru

deeper localization was attributed to weaker quantum confinement in the enlarged localization volume. Nishi *et al.* [12] proposed a completely different reason. The effect of DWELL was attributed to a reduction of the mismatch strain, since the (In,Ga)As QW is tetragonally distorted being grown on a thick GaAs substrate. Consequently, the weaker built-in strain provides deeper localizing potential in the QD.

In this paper we show that DWELL provides deeper localization of charge carriers due to a complex action of *three* processes, namely, an increase of the QD volume, change in the QD aspect ratio, and strain redistribution provided by the QW. We decompose the total possible energy benefit of these three contributions and examine the optimal DWELL configuration sustaining coherent interfaces.

We consider the problem of DWELL in the frame of the complex model [10], which takes into account an interplay between the solid mechanics of the built-in strain-stress fields and quantum mechanics of the localized electrons and holes. In this paper we focus on the InAs QDs in GaAs since this system is widely used and a large amount of reliable experimental data is available to verify our calculation results. Indeed, similar results can be obtained for other material systems.

The model geometry utilized here is similar to the one described in Ref. [10]. We consider a pyramidal InAs QD with height H in the growth direction of [001]. The QD is either embedded into bulk GaAs (QDB) or built-in an (In,Ga)As QW of thickness h (DWELL), as shown in Figs. 1(a) and 1(b). The base of the QD in both cases is situated 60 nm below the top surface, which is traction free. The base edges are aligned along the [100] and [010] crystallographic directions. The whole supercell is as large as 100 nm in the x and y directions and 120 nm in the z direction. This geometry of InAs QD is supported by transmission electron microscopy [11,23,24]. The parameters varied in the modeling are the QD base length L , the aspect ratio H/L , the thickness of the (In,Ga)As QW h , and its chemical composition C_{In} .

First, by using the finite-element method (FEM) we solve the problem of continuum mechanics and obtain the strain ε and stress σ fields. Then, we solve the eigenvalue problem of quantum mechanics on the same mesh in a single-band approximation. In this paper we do not analyze the wave functions and solely focus on the eigenvalues of energy for the ground states of the electron and hole in the QD. We do not study any phenomena related to the interband mixing, since it is not inherent for the single-band model. We take into account that the ground state of holes in a pyramidal InAs QD is predominately composed of the heavy-hole band [25]. The model is validated by comparison with the results of the eight-band $k \cdot p$ -model calculations discussed in Ref. [26]. We use a common set

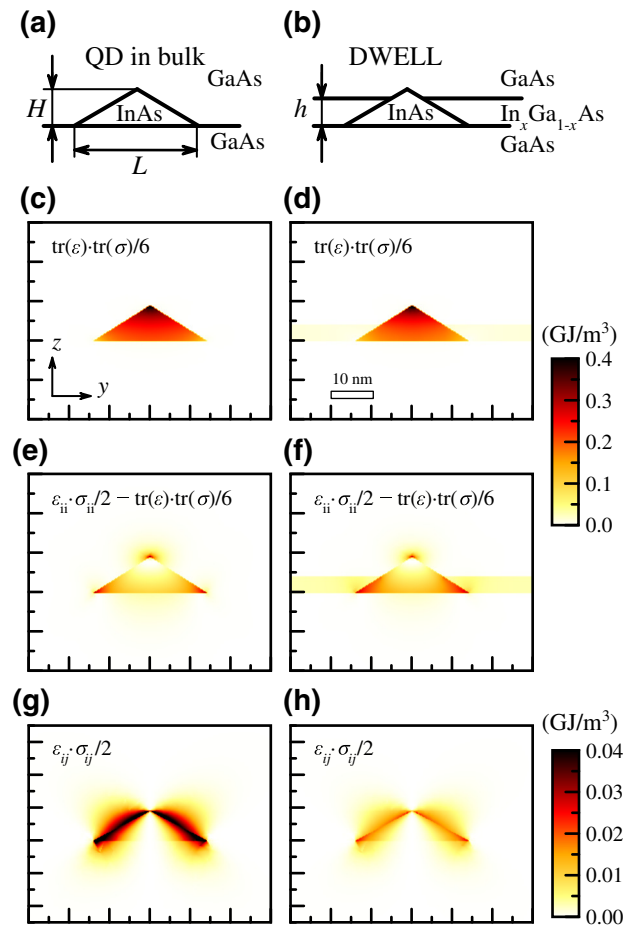


FIG. 1. Comparison of an InAs QD in the bulk GaAs (left column) and InAs DWELL (right column): (a) and (b) sketch of the systems; (c) and (d) density of the hydrostatic energy; (e) and (f) density of the deviatoric energy; (g) and (h) density of the shear energy. The y and z axes are parallel to the crystallographic [010] and [001] directions, correspondingly.

of material parameters [27]. The details of the calculations can be found elsewhere [10].

We decompose the elastic strain ε tensor field into *hydrostatic* (h), *deviatoric* (d), and *shear* (s) components as follows:

$$\begin{aligned}\varepsilon_{ij}^h &= \text{tr}(\varepsilon)\delta_{ij}/3, \\ \varepsilon_{ij}^d &= \varepsilon_{ij}\delta_{ij} - \varepsilon_{ij}^h, \\ \varepsilon_{ij}^s &= \varepsilon_{ij} - \varepsilon_{ij}\delta_{ij},\end{aligned}\quad (1)$$

where δ_{ij} is the Kronecker δ function. The corresponding elastic energy densities can be calculated for each component of the elastic strain-stress field as

$$\begin{aligned}w &= w^h + w^d + w^s = \text{tr}(\varepsilon)\text{tr}(\sigma)/6 \\ &+ [\varepsilon_{ii}\sigma_{ii}/2 - \text{tr}(\varepsilon)\text{tr}(\sigma)/6] + \varepsilon_{ij}\sigma_{ij}/2, i \neq j.\end{aligned}\quad (2)$$

The impact of the decomposed components of the strain-stress field on the localizing potential is different [28]. The hydrostatic compression increases the band gap of (In,Ga)As, so that $\Delta E_c = a_c \text{tr}(\varepsilon)$, $\Delta E_v = a_v \text{tr}(\varepsilon)$, where the deformation potentials for electrons and holes $a_c < 0$, $a_v > 0$ and $|a_c| \gg a_v$. The deviatoric and shear strains split the hole band $\Delta E_v = \pm b \sqrt{-3 \text{inv}_2(\varepsilon^d)}$ and $\Delta E_v = \pm d \sqrt{-\text{inv}_2(\varepsilon^s)}$, where $\text{inv}_2(\varepsilon^{d,s})$ denotes the second invariant of the corresponding strain component tensor.

Figure 1 shows the maps of the elastic energy densities related to the hydrostatic (c) and (d), deviatoric (e) and (f), and shear (g) and (h) strains for the cases of QDB (c), (e), and (g) and DWELL (d), (f), and (h). The cross-section plane is (100) at $x = 0$. Only the middle portion of the supercell is plotted. For both cases the QD height $H = 9$ nm and its base $L = 28$ nm, which corresponds to the experimental observations of InAs QDs self-organized by the Stranski-Krastanow technique and overgrown by a thick GaAs cap [23]. The thickness of the (In,Ga)As QW $h = 3.85$ nm and the indium concentration $C_{\text{In}} = 0.3$ molar fraction. The QWs with these parameters were utilized in Refs. [11,12] to achieve the deepest localization of carriers in DWELLS.

The elastic energy of the QW corresponds to the biaxial strain with two components, hydrostatic and deviatoric, seen as yellow stripes in Figs. 1(d) and 1(f). These energy densities can be, of course, calculated analytically for a prescribed C_{In} , which defines an eigen-strain due to the lattice mismatch between (In,Ga)As and GaAs $\varepsilon_m = (a_{(\text{In,Ga)As}} - a_{\text{GaAs}})/a_{(\text{In,Ga)As}}$. The corresponding elastic coefficients can be defined for (In,Ga)As in linear approximations. Then, for the (In,Ga)As QW parallel to the (001) plane we have the bulk modulus $K = (c_{11} + 2c_{12})/3$, biaxial modulus $M = c_{11} + c_{12} - 2c_{12}^2/c_{11}$, and Poisson's ratio $\nu = c_{12}/(c_{11} + c_{12})$. Both analytical and model calculations give the hydrostatic energy density $w_{\text{QW}}^h \approx 0.015$ GJ/m³ in the considered QW with $C_{\text{In}} = 0.3$ and the deviatoric energy density $w_{\text{QW}}^d \approx 0.03$ GJ/m³. The shear energy for a bare QW is 0.

The distribution of the elastic strain and corresponding energy within the QD is not uniform. It is qualitatively similar for the QDB and DWELL. The highest hydrostatic energy density corresponds to the QD top, where it reaches 0.45 GJ/m³. This quantity is the same for the QDB and DWELL in the configuration depicted in Fig. 1, when the QW does not cover the QD top. The hydrostatic energy density gradually reduces from the top to the base, where $w_{\text{QDB}}^h \approx 0.2$ GJ/m³ and $w_{\text{DWELL}}^h \approx 0.18$ GJ/m³. The integration over the pyramid volume shows that the hydrostatic energy reduces in total from 0.51 fJ (QDB) to 0.45 fJ (DWELL).

The densities of the deviatoric energy plotted in Figs. 1(e) and 1(f) are mostly concentrated near the pyramid base for both cases. $w_{\text{QDB}}^d \approx 0.08$ GJ/m³ in the center

and $w_{\text{QDB}}^d \approx 0.23$ GJ/m³ in the corners. The deviatoric energy rapidly reduces to the pyramid's top, where the QD has mostly hydrostatic strain, but induces a spot of deviatoric strain in the surrounding GaAs matrix. Although the QDB and DWELL show similar distribution of the deviatoric energy inside the QD, there are quantitative differences: $w_{\text{DWELL}}^d \approx 0.1$ GJ/m³ in the center of the pyramid base and $w_{\text{DWELL}}^d \approx 0.25$ GJ/m³ in the corner. The deviatoric energy integrated over the QD volume differs by 25% being 0.24 fJ in the QDB and 0.32 fJ in the DWELL.

The densities of the shear energy plotted in Figs. 1(g) and 1(h) are mostly concentrated near the QD edges. The total shear energy integrated over the QD in both QDB and DWELL cases appeared to be small compared to the hydrostatic and deviatoric energies. Note, the scale for w^s in (g) and (h) is smaller by an order of magnitude compared to the panels for w^h and w^d . The shear component mostly presents within a very close vicinity of the QD sides, while it is sufficiently weaker around the bottom. For the QDB the highest energy density is around 0.04 GJ/m³. In the DWELL case, the shear-strain distribution is similar, but its energy density is 2.5 times smaller.

For the geometries considered above, a numerical solution to the quantum-mechanical problem with the determined strain-stress fields shows that the localization of both electrons and holes is deeper in DWELL than in QDB. The corresponding redshift of the optical excitonic emission is 52 meV. This quantity is substantially less than the experimentally observed value of 140–160 meV [11,12]. The discrepancy indicates that we should consider changes in the QD shape and volume in addition to the QW-induced modification in the strain-stress field in order to quantitatively describe the effect of DWELL.

Before consideration of these additional effects, let us analyze what values of the QW parameters, i.e., h and C_{In} , provide the deepest localization of carriers in a given QD. Obviously, higher C_{In} may provide stronger modification of the strain-stress field in the QD. Thicker QW may expand this modification over the whole volume of the QD including the top portion of it.

An increase of the QW thickness h and indium concentration C_{In} results in the increase of the elastic energy due to either larger lattice mismatch or bigger stressed volume. When elastic energy overcomes a certain threshold, it causes the formation of misfit dislocations. The critical parameters can be determined from the Matthews-Blakeslee formula [29]

$$\frac{b_x^2 + b_y^2 + (1 - \nu)b_z^2}{8\pi(1 + \nu)b_x h_{\text{cr}}} \ln \frac{\alpha h_{\text{cr}}}{b} = \varepsilon_m, \quad (3)$$

where b_x, b_y, b_z are the components of the Burgers vector, b/α is the core cutoff radius of the dislocation. In the calculations, we consider dislocations with the Burgers vector $\frac{1}{2}\langle 110 \rangle$ inclined at 60° to the dislocation line

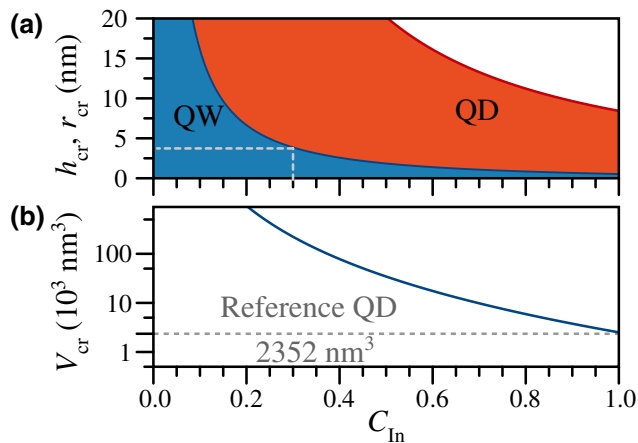


FIG. 2. (a) Dependence of the critical height h_{cr} of the QW and radius r_{cr} of a spherical nanoinclusion on the In concentration; (b) critical volume of an (In,Ga)As QD as a function of the In concentration.

and at 45° to (001). Such dislocations are responsible for the relaxation process in GaAs or (In,Ga)As films [29,30]. A blue field in Fig. 2(a) shows the region of h and C_{In} where a dislocation-free (In,Ga)As QW is thermodynamically stable on the GaAs substrate with (001) orientation. The parameters marked by the gray dashed lines were used in Refs. [11,12] and in our calculations described above to show the concept.

Plotted in Fig. 3 are the results of the quantum-mechanical calculations of the ground-state energies of an electron, hole, and exciton localized in the DWELL. The parameters are as follows. The InAs QD height is 9 nm, its base is 18 (red circles), 28 (green diamonds), or 38 nm (blue triangles). The indium concentration in the QW varies along the horizontal axis from 0 (QDB case) to 0.7. The QW thickness h for each C_{In} is taken equal to the critical value prescribed by Eq. (3). For the sake of greater clarity, we also make calculations for an InAs QD with 28 nm base and 9 nm height, which is fully covered by the QW so that the thermodynamic limitation of the interface coherency is ignored. The results of these calculations are plotted by black open circles and dashed lines.

It follows from Fig. 3 that the localization of both electrons and holes in the QD becomes deeper with growing C_{In} in the QW due to strengthening the modification of the stress-strain field. However, the requirement of the QW interface coherency prescribes smaller thickness of the QW with higher C_{In} , so that the QD is mostly outside the layer where the strain field is modified by the QW. As a trade-off between the strength of the effect and the volume affected, the optimal QW parameters are $C_{In} = 0.3$, $h = 3.85$ nm for all the base lengths. It is worthwhile to note that this set of the QW parameters was experimentally found as the most efficient DWELL configuration in Refs. [11,12,20–22].

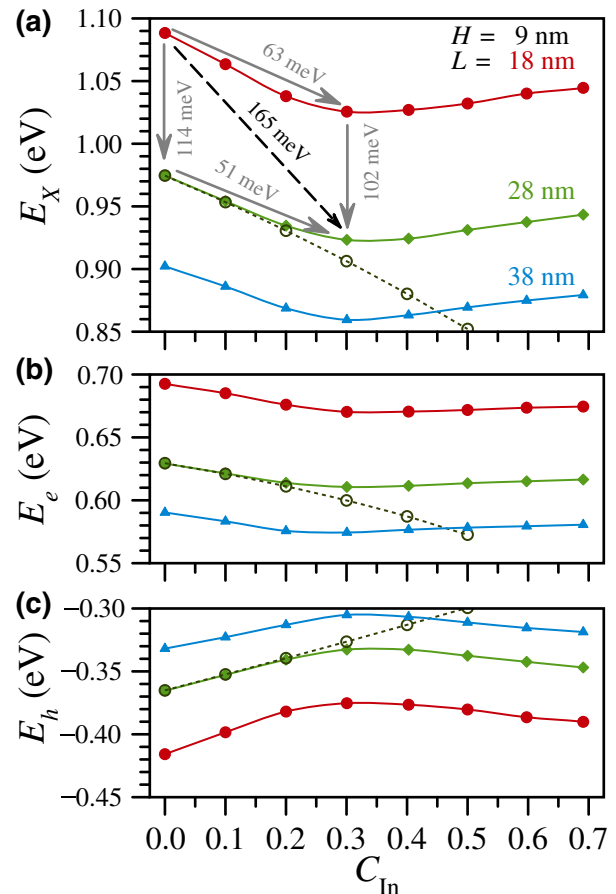


FIG. 3. Energies of (a) exciton, (b) electron, and (c) heavy hole localized in the InAs QDs versus In concentration in the (In,Ga)As QWs. The QD height is 9 nm. Green, red, and blue curves and dots correspond to the QD base of 18, 28, and 38 nm. Solid lines and symbols are calculated for the QW thickness defined by Eq. (3). Open circles and dashed lines are calculated for the QW thickness equal to the QD height.

The three curves in each panel of Fig. 3 have the following rationale. First, the well-developed InAs QDs on the GaAs surface usually have {101} facets [31], which corresponds to the pyramid aspect ratio $H/L = 0.5$ and the base length $L = 18$ nm if $H = 9$ nm. Second, the QD volume and shape are changed during the overgrowth by the barrier material [31–34]. For InAs QDs overgrown by GaAs a precise transmission electron microscopy revealed {203} facets [23], which corresponds to the pyramid aspect ratio $H/L = 0.32$ and the base length $L = 28$ nm if $H = 9$ nm. Third, the analysis carried out in Ref. [10] showed that the optimal aspect ratio of approximately 0.2 provides the deepest carrier localization in an InAs QD of any given volume buried in GaAs. We take $L = 38$ nm for calculations, which corresponds to $H/L = 0.24$ if $H = 9$ nm.

It should be noted that although a low aspect ratio is thermodynamically favorable for buried QDs [10], the

actual aspect ratio depends on the growth kinetics, i.e., on the technological procedure. In the case of bare QDs, the reduction of the aspect ratio occurs with a constant QD volume, since there is no external source of indium atoms when the GaAs top barrier is deposited. In the case of DWELL there is a lot of indium available for the QD base extension during the deposition of the (In,Ga)As QW. In this case, the change of the base length should happen with almost constant QD height H . This statement is supported by the TEM study when InAs QDB and DWELL are compared [11,24].

The total elastic energy of a QD is proportional to its volume, which grows with the increasing base length and constant height of the pyramid. When certain critical volume is reached, the elastic energy should relax by the formation of misfit dislocation loops. An analytical consideration of a spherical QD leads [9,35] to a formula for r_{cr} similar to Eq. (3) for h_{cr}

$$\frac{3b}{4\pi(1+\nu)r_{cr}} \ln \frac{\alpha r_{cr}}{b} \approx \varepsilon_m. \quad (4)$$

The dependence of $r_{cr}(C_{In})$ is shown in Fig. 2(a) by the red curve where the colored region corresponds to dislocation-free interfaces. The corresponding critical volume of the QD is plotted as a function of C_{In} in Fig. 2(b). It follows from the calculations that for InAs QD (i.e., $C_{In} = 1$) the critical volume is close to the volume of a pyramid with a height $H = 9$ nm and base $L = 28$ nm ($V = 2352$ nm³). The QDs with larger bases are thermodynamically unstable against the formation of misfit dislocations. For instance, the QD with a height of 9 nm and a base length of 38 nm has the volume 2 times larger than the critical one.

So, the requirements of the interface coherency impose a strong limitation on the QD and QW composition and geometry. It sets the limit of an improvement of the carrier localization in the DWELL compared to the bare QD. The largest redshift of the excitonic emission from a pyramidal InAs QD with the height $H = 9$ nm is shown in Fig. 3 by the dashed arrow. It corresponds to the 3.85-nm-thick QW with $C_{In} = 0.3$. The same configuration of DWELL was experimentally found to be the most efficient [11,12]. The calculated shift of the excitonic emission by 165 meV is well consistent with the experimental achievement by Ustinov *et al.* (160 meV) [11].

For deeper insight into the phenomenon, let us decompose the total value of the redshift into the contributions related to the modification of the strain-stress field due to QW, increase of the QD volume and change in the QD aspect ratio. The former can be evaluated from Fig. 3 as a difference $E_X(C_{In} = 0) - E_X(C_{In} = 0.3) = (51 \div 63)$ meV.

In order to resolve the volume and aspect ratio contributions, we vary the latter while the QD volume remains constant. The results of calculations of the energies of

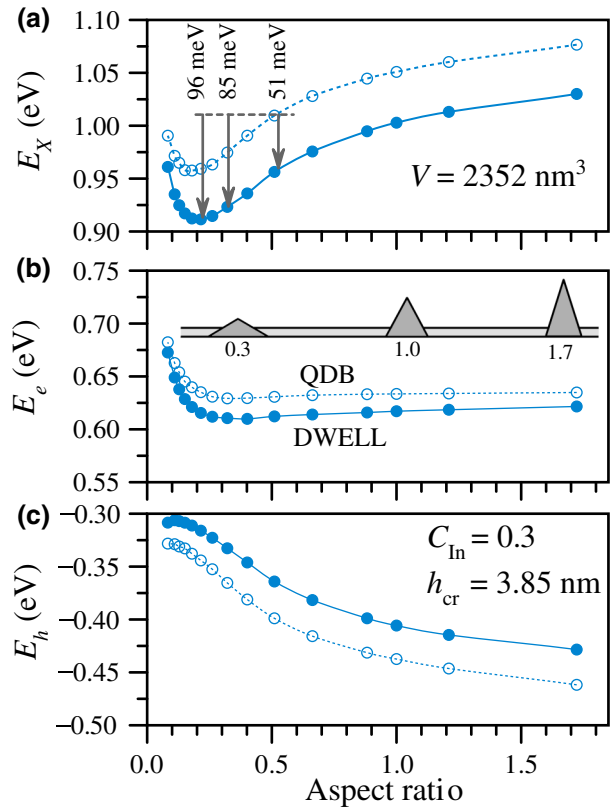


FIG. 4. Energies of the (a) exciton, (b) electron, and (c) heavy hole as functions of the aspect ratio of the pyramidal InAs QD with constant volume. Full and open circles correspond to the DWELL and QDB cases, respectively.

localized electrons (E_e), holes (E_h), and excitons (E_X) are shown in Fig. 4. The volume of the reference InAs QDs is 2352 nm³. In Fig. 3 it corresponds to the green lines for the QD with $H = 9$ nm and $L = 28$ nm. The blue full circles in Fig. 4 represent the case of DWELL with the (In,Ga)As QW of thickness $h = 3.85$ nm and with $C_{In} = 0.3$. The open circles represent the case of a bare InAs QD in the bulk GaAs. For both cases, the dependencies of the carrier energies on the aspect ratio are similar with the shift by 51 meV discussed above. An interplay of quantum mechanics and solid mechanics provides a pronounced minimum of the exciton energy when the aspect ratio is near 0.2 for both QDB and DWELL. The aspect ratio experimentally observed by Ustinov *et al.* in the case of DWELL was 0.32. The decrease of the exciton energy in DWELL is 34 meV when the aspect ratio is reduced from 0.5 to 0.32. The total redshift of the excitonic state equals 85 meV when the QD volume remains unchanged. Farther reshaping to the optimal aspect ratio could give an additional redshift of the exciton energy by 11 meV to total 96 meV.

Thus, we separate the contributions of the volume and aspect ratio (approximately 78 and 36 meV,

correspondingly) in the redshift of 114 meV accompanying an increase of the base L from 18 to 28 nm during the (In,Ga)As QW deposition. With the additional 51 meV due to the redistribution of the strain-stress field, the total improvement of the exciton localization is as large as 165 meV. This value is in a very good quantitative agreement with the best experimental achievements [11,12].

Our calculations predict the limit of improvement of the exciton localization for the InAs-GaAs DWELL system when compared to the InAs QDB, it is as large as 176 meV. When the QD volume is strictly limited by the requirements of the interface coherency, the strongest possible localization of carriers can be achieved if the optimal QD aspect ratio of approximately 0.2 is obtained during the overgrowth procedure. We note that flatter of the QD during overgrowth is thermodynamically favorable [10] and, therefore, possible.

There are several phenomena such as In-Ga intermixing and alloy fluctuations, which can change the layout of the model. In accord to the TEM observations [11] these phenomena make a minor impact under common growth procedure, however, they should become relevant in cases of a high-temperature treatment or strongly nonequilibrium growth. Such cases deserve special consideration, which is out of the scope of this paper.

In conclusion, we study charge-carrier localization by a pyramidal QD, which can be enhanced when the QD is embedded in a QW. We reveal that three processes contribute to the effect, namely, modification of the strain-stress field, an increase of the QD volume, and decrease of the QD aspect ratio. The total effect is limited by the requirements of the interface coherency for both QD and QW. We analyze the strain-stress field and the coherency conditions for the most popular DWELL composed of InAs QD and (In,Ga)As QW. For this system, a very good quantitative agreement is achieved between our calculation results and the available experimental data. In optimal DWELL configuration, the total effect of (In,Ga)As QW on the carrier localization in the InAs QD can be as large as 176 meV in terms of the redshift of the localized exciton energy. We decompose this redshift of the exciton energy into three components, corresponding to the increase of the QD volume (78 meV), reduction of the QD aspect ratio (47 meV), and QW driven strain-stress field redistribution (51 meV). Evidently, all the three contributions are valuable for the phenomenon.

Our results are qualitatively valid and can readily be adopted to any similar DWELL systems, such as InAs-InP, GaSb-AlAs, etc.

ACKNOWLEDGMENTS

We wish to thank N. Cherkashin, A. Kononov, and S. Kukhtaruk for useful discussions. We thank A. Ilina

for carefully reading the manuscript. This research is supported by the Russian Foundation for Basic Research, Project No. 19-32-90116.

- [1] Z. I. Alferov, Nobel lecture: The double heterostructure concept and its applications in physics, electronics, and technology, *Rev. Mod. Phys.* **73**, 767 (2001).
- [2] K. E. Sautter, K. D. Vallejo, and P. J. Simmonds, Strain-driven quantum dot self-assembly by molecular beam epitaxy, *J. Appl. Phys.* **128**, 031101 (2020).
- [3] S. Michaelis de Vasconcellos, S. Gordon, M. Bichler, T. Meier, and A. Zrenner, Coherent control of a single exciton qubit by optoelectronic manipulation, *Nat. Photonics* **4**, 545 (2010).
- [4] A. N. Kosarev, H. Rose, S. V. Poltavtsev, M. Reichelt, C. Schneider, M. Kamp, S. Höfling, M. Bayer, T. Meier, and I. A. Akimov, Accurate photon echo timing by optical freezing of exciton dephasing and rephasing in quantum dots, *Commun. Phys.* **3**, 1 (2020).
- [5] New Semiconductor Materials. Characteristics and Properties, <http://www.ioffe.ru/SVA/NSM/Semicond/index.html>.
- [6] O. Stier and D. Bimberg, Modeling of strained quantum wires using eight-band kp theory, *Phys. Rev. B* **55**, 7726 (1997).
- [7] M. Y. Petrov, I. V. Ignatiev, S. V. Poltavtsev, A. Greilich, A. Bauschulte, D. R. Yakovlev, and M. Bayer, Effect of thermal annealing on the hyperfine interaction in InAs/GaAs quantum dots, *Phys. Rev. B* **78**, 045315 (2008).
- [8] I. N. Stranski and L. Krastanow, Zur Theorie der orientierten Ausscheidung von Ionenkristallen aufeinander, *Monatshefte für Chemie und Verwandte Teile Anderer Wissenschaften* **71**, 351 (1937).
- [9] V. V. Chaldyshev, N. A. Bert, A. L. Kolesnikova, and A. E. Romanov, Stress relaxation scenario for buried quantum dots, *Phys. Rev. B* **79**, 233304 (2020).
- [10] A. Kosarev and V. V. Chaldyshev, Carrier localization in self-organized quantum dots: An interplay between quantum and solid mechanics, *Appl. Phys. Lett.* **117**, 202103 (2020).
- [11] V. M. Ustinov, N. A. Maleev, A. E. Zhukov, A. R. Kovsh, A. Y. Egorov, A. V. Lunev, B. V. Volovik, I. L. Krestnikov, Y. G. Musikhin, N. A. Bert, P. S. Kop'ev, Z. I. Alferov, N. N. Ledentsov, and D. Bimberg, InAs/InGaAs quantum dot structures on GaAs substrates emitting at 1.3 μm , *Appl. Phys. Lett.* **74**, 2815 (1999).
- [12] K. Nishi, H. Saito, S. Sugou, and J. Lee, A narrow photoluminescence linewidth of 21 meV at 1.35 μm from strain-reduced InAs quantum dots covered by In_{0.2}Ga_{0.8}As grown on GaAs substrates, *Appl. Phys. Lett.* **74**, 1111 (1999).
- [13] H. Y. Liu, I. R. Sellers, T. J. Badcock, D. J. Mowbray, M. S. Skolnick, K. M. Groom, M. Gutiérrez, M. Hopkinson, J. S. Ng, J. P. R. David, and R. Beanland, Improved performance of 1.3 μm multilayer InAs quantum-dot lasers using a high-growth-temperature GaAs spacer layer, *Appl. Phys. Lett.* **85**, 704 (2004).
- [14] Y. B. Ezra and B. I. Lembrikov, Synchronized carrier dynamics in quantum dot-in-a-well (QDWELL) laser under an optical injection, *IEEE J. Sel. Top. Quantum Electron.* **19**, 1 (2013).

- [15] Y. B. Ezra and B. I. Lembrikov, Quantum dot-in-a-well (QDWELL) laser dynamics under optical injection, *Opt. and Quantum Electron.* **46**, 1239 (2014).
- [16] S. Wolde, Y. Lao, A. G. Unil Perera, Y. H. Zhang, T. M. Wang, J. O. Kim, T. Schuler-Sandy, Z. Tian, and S. Krishna, Noise, gain, and capture probability of p-type InAs-GaAs quantum-dot and quantum dot-in-well infrared photodetectors, *J. Appl. Phys.* **121**, 244501 (2017).
- [17] T. Torchynska, R. Cisneros-Tamayo, L. Vega-Macotela, G. Polupan, and A. Escobosa-Echavarria, Emission and HR-XRD study of MBE structures with InAs quantum dots and AlGaInAs strain reducing layers, *Superlattices Microstruct.* **124**, 153 (2018).
- [18] S. Asahi, T. Kaizu, and T. Kita, Adiabatic two-step photoexcitation effects in intermediate-band solar cells with quantum dot-in-well structure, *Sci. Rep.* **9**, 7859 (2019).
- [19] W. Li, S. Chen, J. Wu, A. Li, M. Tang, L. Yang, Y. Chen, A. Seeds, H. Liu, and I. Ross, The effect of post-growth rapid thermal annealing on InAs/InGaAs dot-in-a-well structure monolithically grown on Si, *J. Appl. Phys.* **125**, 13530 (2019).
- [20] Z. Niu, X. Wang, Z. Miao, and S. Feng, Modification of emission wavelength of self-assembled In(Ga)As/GaAs quantum dots covered by $\text{In}_x\text{Ga}_{1-x}\text{As}$ ($0 \leq x \leq 0.3$) layer, *J. Cryst. Growth* **227–228**, 1062 (2001).
- [21] H. Y. Liu, X. D. Wang, J. Wu, B. Xu, Y. Q. Wei, W. H. Jiang, D. Ding, X. L. Ye, F. Lin, J. F. Zhang, J. B. Liang, and Z. G. Wang, Structural and optical properties of self-assembled InAs/GaAs quantum dots covered by $\text{In}_x\text{Ga}_{1-x}\text{As}$ ($0 \leq x \leq 0.3$), *J. Appl. Phys.* **88**, 3392 (2000).
- [22] J. Tatebayashi, M. Nishioka, and Y. Arakawa, Over $1.5\mu\text{m}$ light emission from InAs quantum dots embedded in InGaAs strain-reducing layer grown by metalorganic chemical vapor deposition, *Appl. Phys. Lett.* **78**, 3469 (2001).
- [23] N. Cherkashin, S. Reboh, M. J. Hÿtch, A. Claverie, V. V. Preobrazhenskii, M. A. Putyato, B. R. Semyagin, and V. V. Chaldyshev, Determination of stress, strain, and elemental distribution within In(Ga)As quantum dots embedded in GaAs using advanced transmission electron microscopy, *Appl. Phys. Lett.* **102**, 173115 (2013).
- [24] S. Ruvimov, P. Werner, K. Scheerschmidt, U. Gösele, J. Heydenreich, U. Richter, N. N. Ledentsov, M. Grundmann, D. Bimberg, V. M. Ustinov, A. Y. Egorov, P. S. Kop'ev, and Z. I. Alferov, Structural characterization of (In, Ga)As quantum dots in a GaAs matrix, *Phys. Rev. B* **51**, 14766 (1995).
- [25] O. Stier, *Theory of the Electronic and Optical Properties of InGaAs/GaAs Quantum Dots* (Springer, Berlin, 2002).
- [26] O. Stier, M. Grundmann, and D. Bimberg, Electronic and optical properties of strained quantum dots modeled by 8-band kp theory, *Phys. Rev. B* **59**, 5688 (1999).
- [27] S. Adachi, *Properties of Semiconductor Alloys: group-IV, III-V and II-VI Semiconductors* (John Wiley & Sons, New York, 2009).
- [28] G. L. Bir and G. E. Pikus, *Symmetry and Deformation Effects in Semiconductors* (John Wiley & Sons, New York, 1974).
- [29] J. W. Matthews and A. E. Blakeslee, Defects in epitaxial multilayers: I. Misfit dislocations, *J. Cryst. Growth* **27**, 118 (1974).
- [30] N. A. Bert, A. L. Kolesnikova, V. N. Nevedomsky, V. V. Preobrazhenskii, M. A. Putyato, A. E. Romanov, V. M. Seleznev, B. R. Semyagin, and V. V. Chaldyshev, Formation of dislocation defects in the process of burying of InAs quantum dots into GaAs, *Semiconductors* **43**, 1387 (2009).
- [31] P. Kratzer, Q. K. K. Liu, P. Acosta-Diaz, C. Manzano, G. Costantini, R. Songmuang, A. Rastelli, O. G. Schmidt, and K. Kern, Shape transition during epitaxial growth of InAs quantum dots on GaAs(001): Theory and experiment, *Phys. Rev. B* **73**, 205347 (2006).
- [32] I. Daruka, J. Tersoff, and A. Barabási, Shape Transition in Growth of Strained Islands, *Phys. Rev. Lett.* **82**, 2753 (1999).
- [33] R. Songmuang, S. Kiravittaya, and O. Schmidt, Shape evolution of InAs quantum dots during overgrowth, *J. Cryst. Growth* **249**, 416 (2003).
- [34] Y. Tu and J. Tersoff, Coarsening, Mixing, and Motion: The Complex Evolution of Epitaxial Islands, *Phys. Rev. Lett.* **98**, 096103 (2007).
- [35] A. L. Kolesnikova, A. E. Romanov, and V. V. Chaldyshev, Elastic-energy relaxation in heterostructures with strained nanoinclusions, *Phys. Solid State* **49**, 667 (2007).